Cell Reports, Volume *15*

Supplemental Information

Translaminar Cortical Membrane Potential Synchrony in Behaving Mice

Wen-Jie Zhao, Jens Kremkow, and James F.A. Poulet

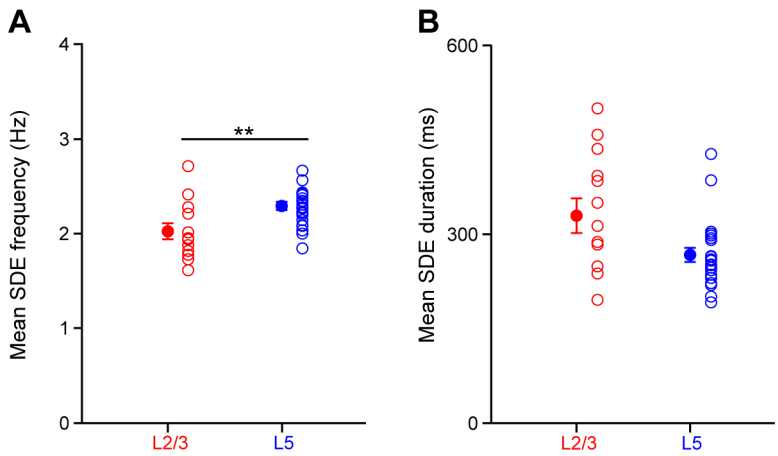

Figure S1, related to Figure 2. Characterization of slow depolarizing events during quiet wakefulness.

(A) Mean frequency of slow depolarizing events (SDE) during quiet wakefulness in L2/3 and L5 neurons. Filled circles with error bars show mean ± SEM. Open circles show individual cells.
(B) Mean duration of SDE's in L2/3 and L5 neurons.

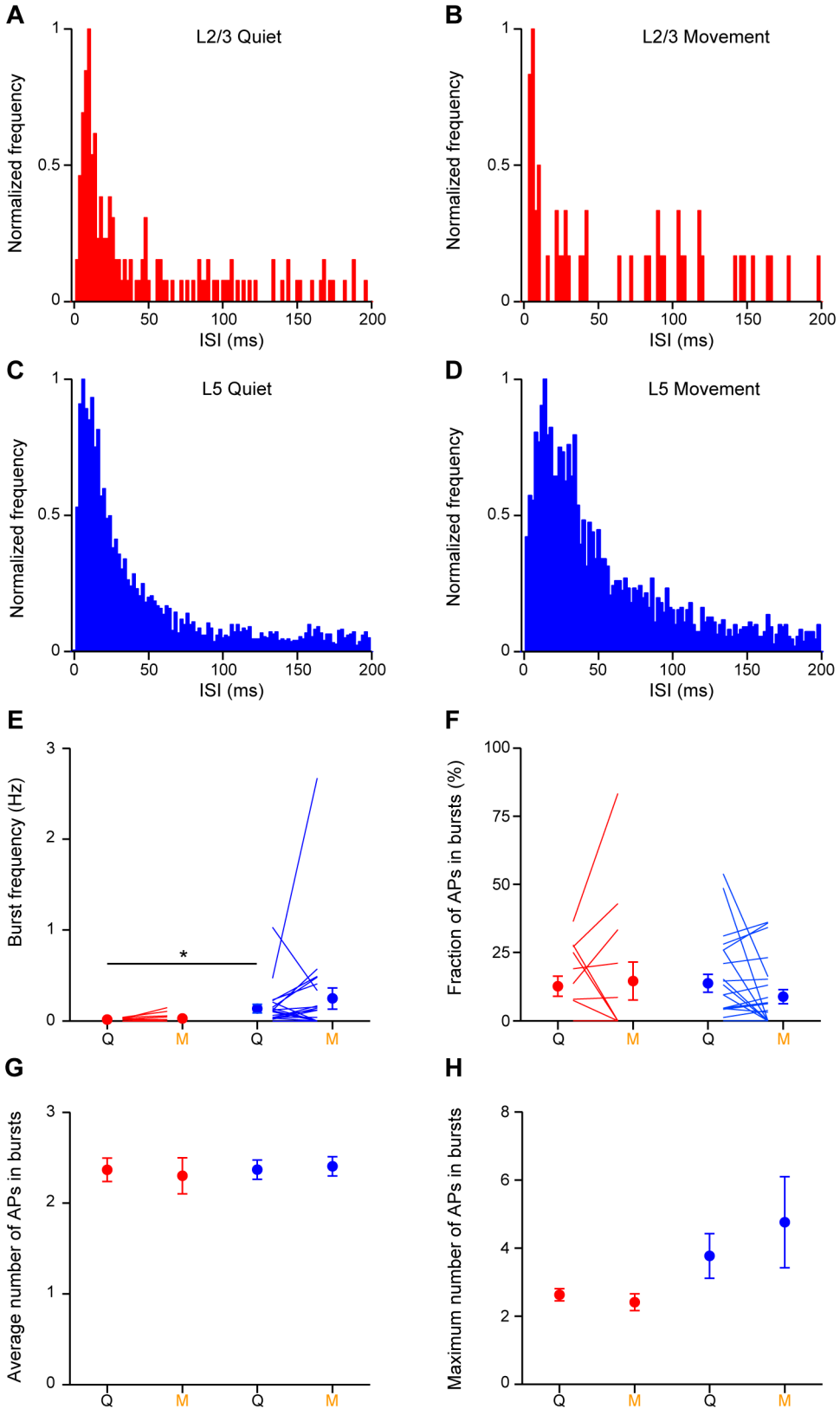

Figure S2, related to Figure 2. Analysis of spontaneous action potential bursting during quiet and moving periods

(A) Inter-spike interval (ISI) distribution of L2/3 neurons during quiet periods.
(B) ISI distribution of L2/3 neurons during moving periods.

(C) Same as (A) but for L5 neurons.
(D) Same as (B) but for L5 neurons.
(E) AP burst frequency in L2/3 and L5 during quiet and moving periods. Filled circles with error bars show mean ± SEM. Lines show individual cells. See methods for burst classification.
(F) Fraction of APs in bursts in L2/3 and L5 during quiet and moving periods.
(G) Mean number of APs in a burst is similar in L2/3 and L5 neurons. Filled circles with error bars show mean ± SEM.
(H) Maximum number of APs in a burst in L2/3 and L5 neurons.

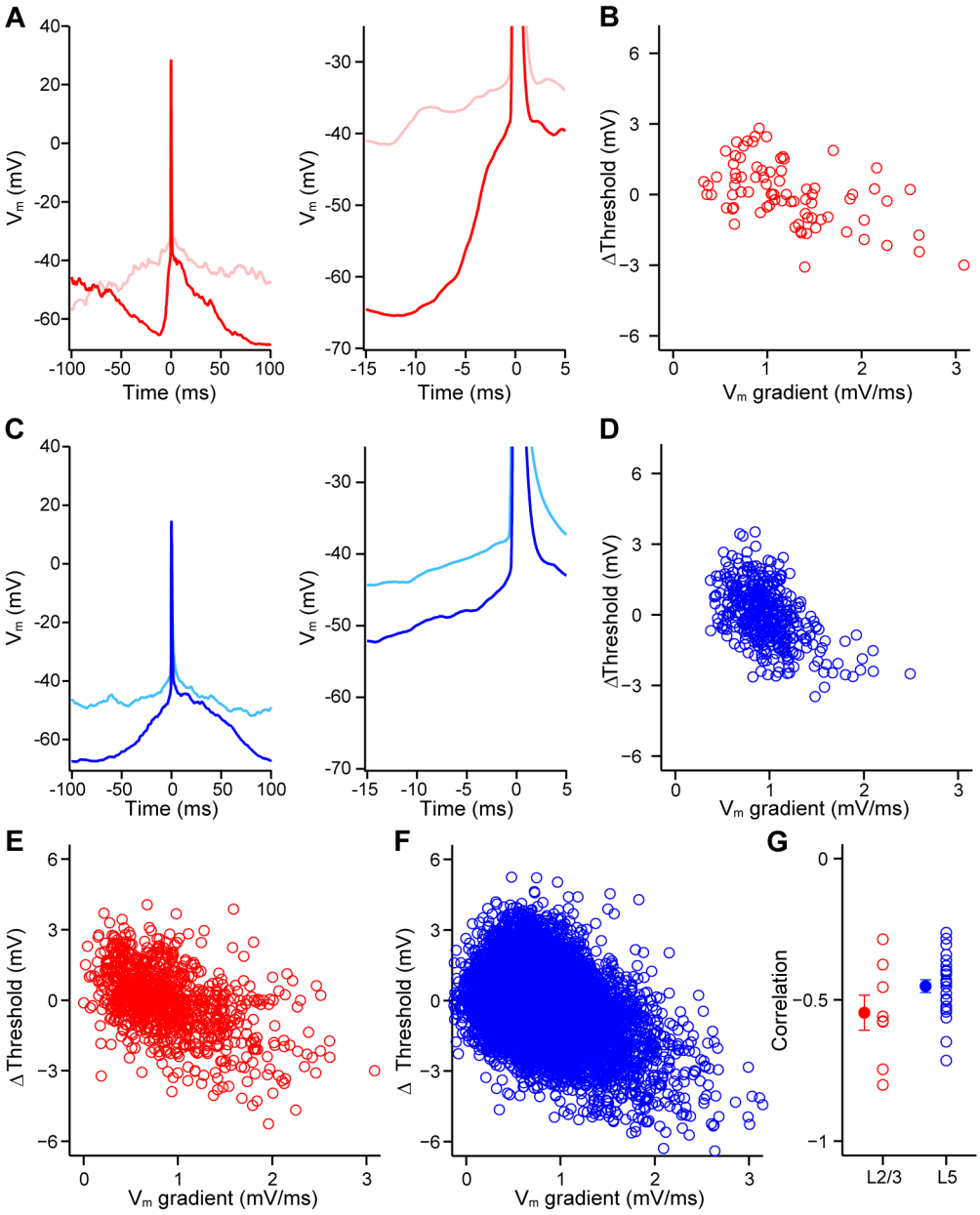

Figure S3, related to Figure 2. Action potential threshold is dependent on the speed of pre-spike depolarization in L2/3 and L5.

(A) Left: two superimposed example action potentials from a L2/3 neuron with different pre-spike V_m rise times. Right: higher temporal resolution image of the example action potentials highlights the dependence of threshold on the pre-spike V_m rise time, with a faster pre-spike depolarization resulting in a lower threshold.
(B) The difference in single spike action potential threshold from the mean action potential threshold, as a function of the gradient of the V_m in the 5 ms before action potential threshold for the example neuron in (A).
(C) Same as (A) but for a L5 neuron.
(D) Same as (B) but for the L5 neuron shown in (C).
(E) Same as (B) but for entire population of L2/3 APs.

(F) Same as (D) but for entire population of L5 APs.
(G) Pearson r correlation coefficient of the change in AP threshold versus the pre-spike V_m gradient, open circles represent individual neurons (L2/3 red, L5 blue).

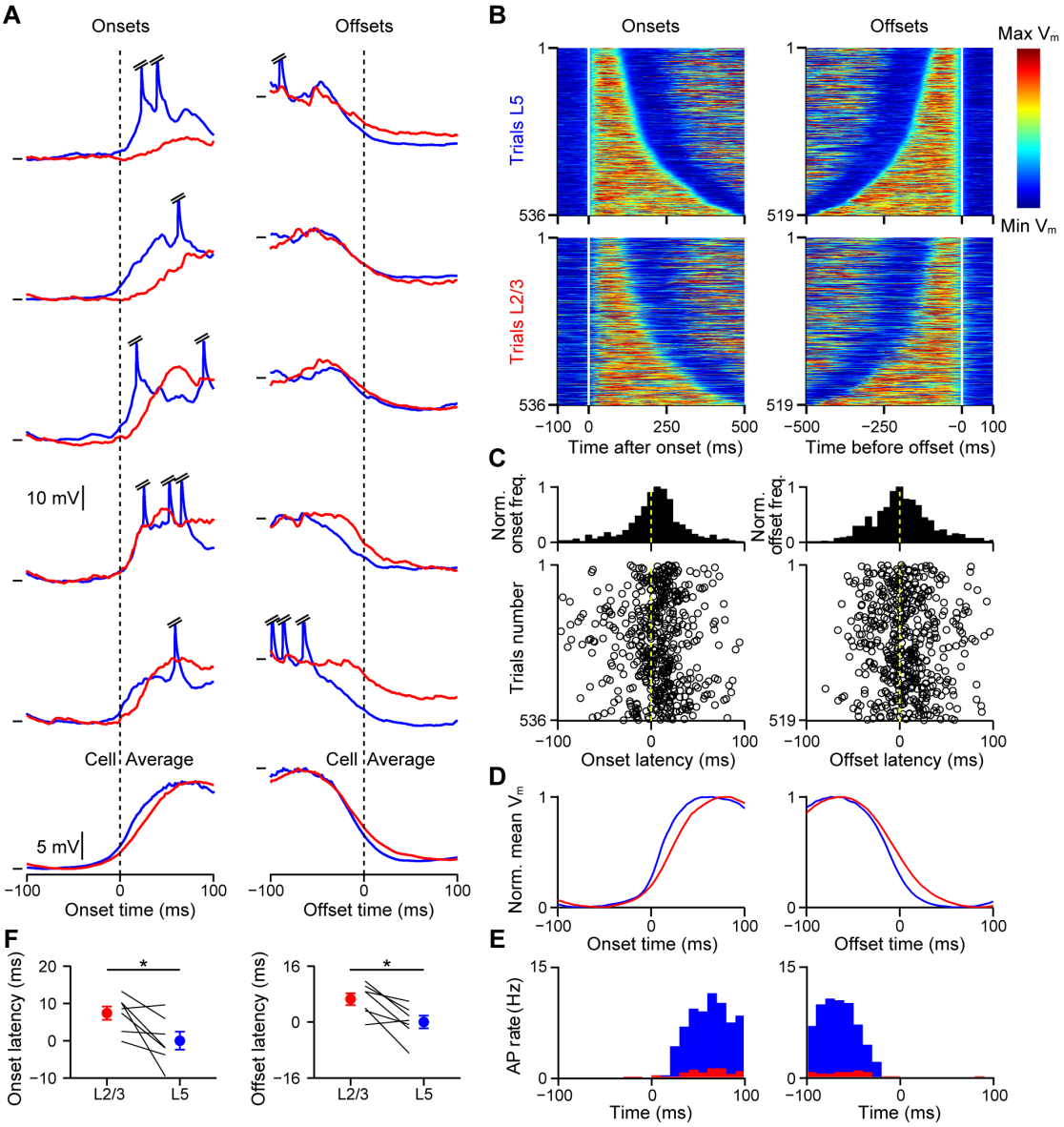

Figure S4, related to Figure 4. L5 triggered slow depolarizing events during quiet wakefulness.

(A) Example SDEs from a dual L2/3 (red) and L5 (blue) whole-cell recording in an awake, resting mouse. V_m traces are aligned to the threshold crossing at onset (left) and offset (right) of the SDE in the L5 neuron, bottom traces show V_m averages. Horizontal lines indicate for L2/3 and L5: trial 1 onset –58.9 / –57.4 mV and offset –44.6 / –39.8 mV; trial 2 onset –59.7 / –57 mV and offset –44.3 / –38.5 mV; trial 3 onset –60.5 / –53.0 mV and offset –48.9 / –44.3 mV; trial 4 onset –58.4 / –47.9 mV and offset –35.2 / –31.2 mV; trial 5 onset –56.7 / –48.4 mV and offset –42.5 / –30.9 mV. Average onset –59.7 / –53.1 mV and offset –43.0 / –37.3 mV. APs have been truncated.
(B) Plots of selected SDEs from 7 dual whole-cell recordings. SDEs were aligned at threshold crossing at the onset (left) and offset (right) of the SDE in the L5 neuron and arranged by duration. Upper boxes show L5 data and lower show L2/3 with colors corresponding to the normalized V_m from minimum (blue) to maximum (red) values.

(C) Population distribution (top) and trial-by-trial measurements (bottom) of the subthreshold onset (left) and offset (right) times in L2/3 neurons relative to the onset and offset times in L5 respectively (n = 7 dual recordings). Onset and offset times were estimated by the 5% level of a sigmoidal fit to the V_m at onset and offset (see Supplemental Experimental Procedures for details).
(D) Population average of the normalized V_m SDEs in L2/3 and L5 relative to the threshold-crossing at onset and offset of the L5 neuron.
(E) Population peri-SDE time histogram of AP times from the dataset in (D).
(F) Population analysis of onset and offset times triggered on the L5 SDE shows significantly earlier onset and offset times in L5. To calculate the onset/offset timing difference, we first measured the time of SDE onset/offset relative to the time of threshold crossing of the L5 SDE. Then we subtracted the population mean L5 onset/offset time from all values. Filled circles with error bars show mean ± SEM, lines show data from individual pairs. For all panels *$p < 0.05$, **$p < 0.01$, ***$p < 0.001$.

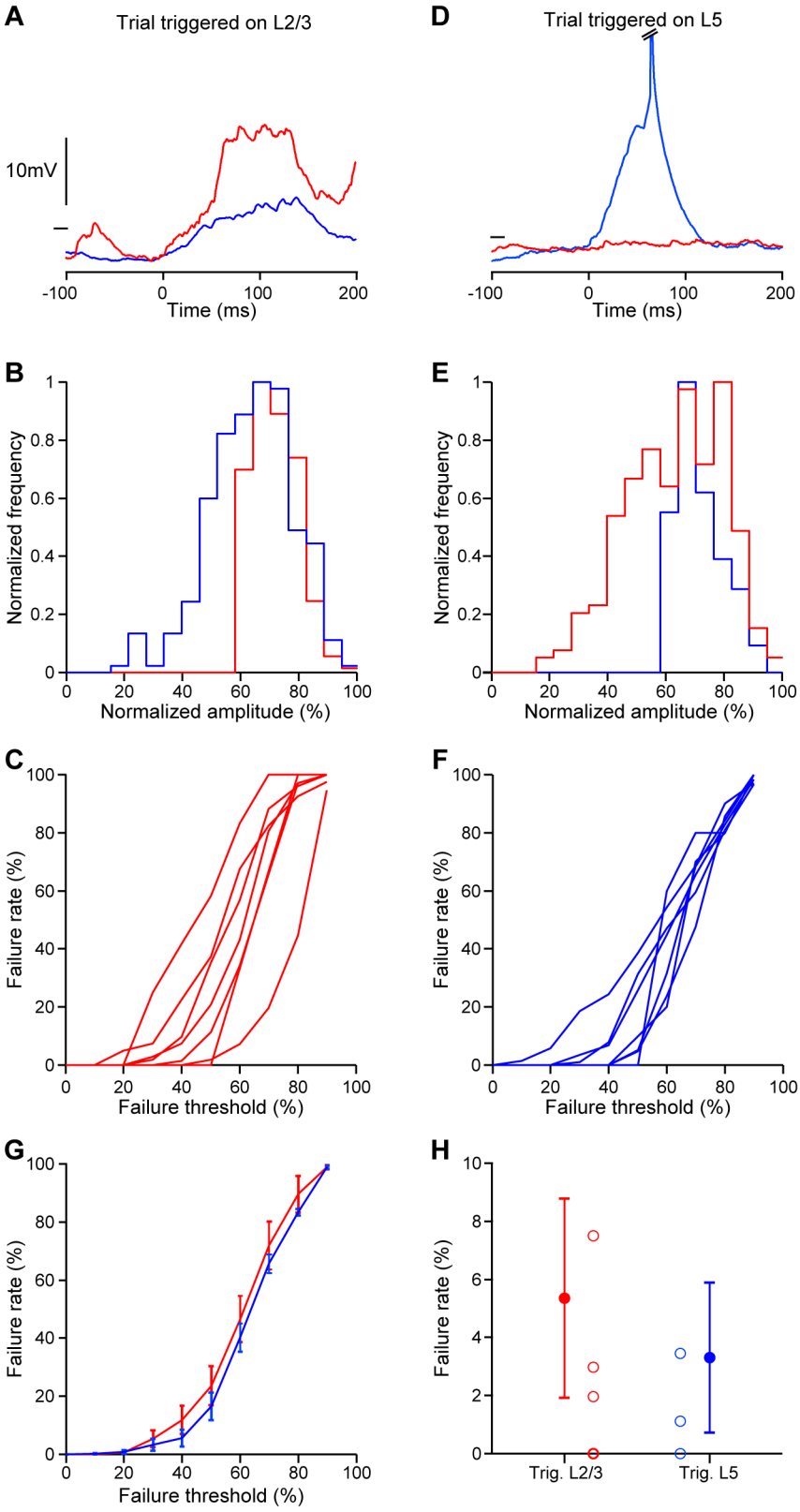

Figure S5, related to Figure 4. Small amplitude slow depolarizing events show occasional failure in other recorded layer.

(A) Example SDE from a dual recording triggered on the L2/3 activity (red) showing low amplitude event in L5 (blue), tick mark shows L5 / L2/3: –60 mV / –65 mV.
(B) Distribution of normalized SDE amplitudes when triggered on L2/3 SDEs larger than 60% of the normalized peak amplitude (see Supplemental Experimental Procedures).
(C) Failure rate as a function of failure threshold when triggering on L2/3. Failure threshold was the SDE amplitude in L5 below which a SDE was counted as a failure.
(D) Same as (A) but triggered on a L5 SDE, tick mark shows L5/L2/3: –60 mV / –68 mV.
(E) Same as (B) but triggered on a L5 SDE.
(F) Same as in (C) but triggered on a L5 SDE. Failure threshold was the SDE amplitude in L2/3 below which a SDE was counted as a failure.
(G) Population averaged failure rates when triggered on L2/3 (red) and L5 (blue).
(H) Failure rates when triggering on different layers at a failure threshold of 30% amplitude.

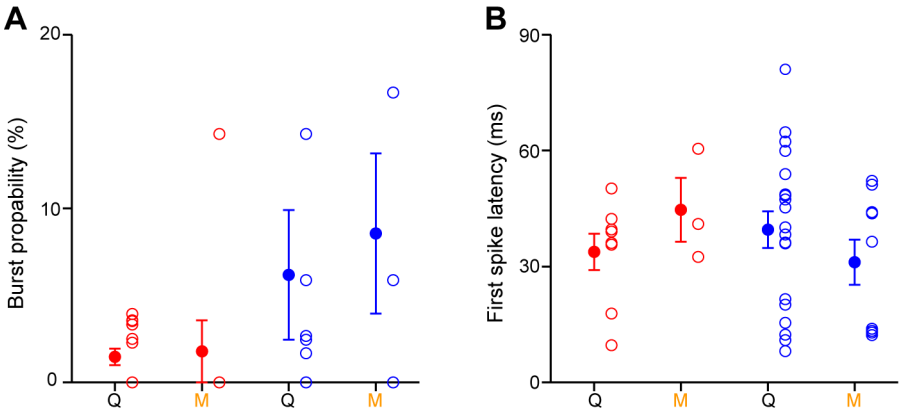

Figure S6, related to Figure 6. Sensory-evoked action potential bursting.

(A) Action potential burst probability during the sensory response in L2/3 and L5 neurons during quiet and moving periods. Burst probability was calculated as the fraction of trials in which a burst was detected in the 100 ms following stimulus onset. Filled circles with error bars show mean ± SEM. Open circles show individual cells.
(B) Sensory-evoked first spike latency was similar in L2/3 and L5 during quiet and moving periods.

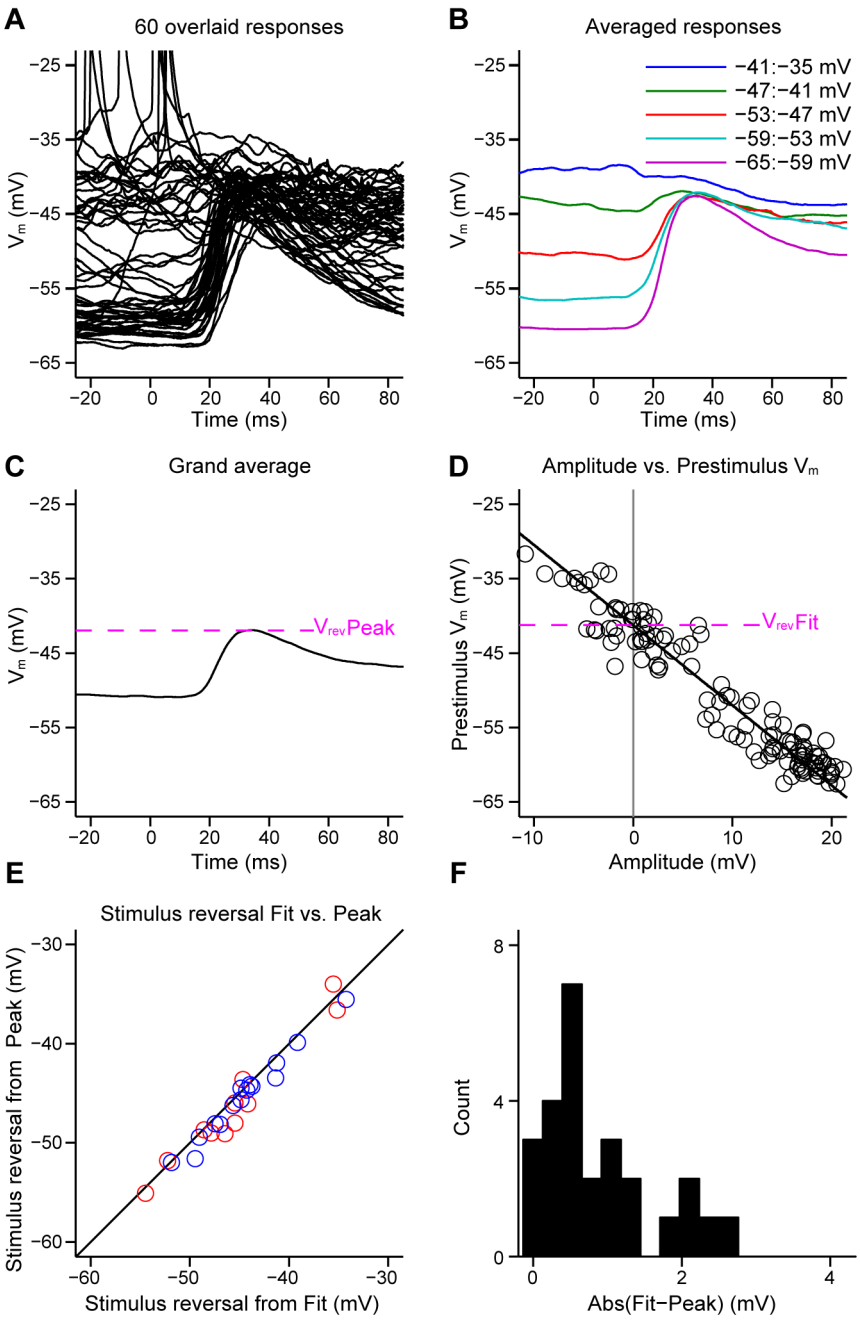

Figure S7, related to Figure 6. Measurement of the tactile stimulus-evoked reversal potential.

(A) Example trial-by-trial V_m responses of a L2/3 cortical neuron to tactile stimulation of the forepaw digits in an awake mouse.
(B) Averaged tactile-evoked responses from neuron in (A) grouped into 5 categories based on the pre-stimulus V_m show a reduced response amplitude at more depolarized V_m values.
(C) Grand average from the example neuron in (A and B), pink dashed line shows the peak V_m of the grand average response ($Vrev_{Peak}$).
(D) Plot of the amplitude of all individual tactile-evoked responses (open circles) from example neuron in (A to C) against the pre-stimulus V_m. Pink

dashed line shows the reversal potential as defined by the point at which the linear fit (black line) crosses the 0 mV tactile-stimulus evoked response amplitude (grey line).
(E) The peak V_m of the average tactile-evoked response (as in C) plotted against the reversal potential as determined by fitting the individual responses (as in D) shows significant correlation across all recorded cells. Red circles show L2/3 cells and blue circles L5 cells.
(F) Distribution of the differences in reversal potential as measured by both methods. The mean distance was 1.00 ± 0.15 mV.

SUPPLEMENTAL EXPERIMENTAL PROCEDURES

Surgery and intrinsic optical imaging

Male 6 to 9 week old C57bl6J mice were anesthetized with isoflurane (1.5 to 2% in O_2) and implanted with a lightweight metal head support. The skull was exposed over forepaw S1 and a recording chamber made from dental cement (Paladure, Heraeus Kulzer). The forepaw representation of digit 3 (D3) was identified with intrinsic optical imaging. D3 was stimulated with a piezo-element at 10 Hz during red light illumination of the skull. The intrinsic optical signal and blood vessel patterns were then used to guide the location of the craniotomies. On the day of the experiment, mice were anesthetized and for single recording experiments, one craniotomy was made over the center of the D3 intrinsic signal. For dual recordings, two < 0.5 mm diameter craniotomies were drilled next to each other, one directly over the center of the D3 intrinsic signal response and the second more lateral to attempt to target L5 and L2/3 neurons in the same column. The exposed brain was covered with Kwik-Cast (WPI) and mice were allowed to recover for > 3 hours following surgery before attempting whole-cell recordings.

Monitoring forepaw movement and tactile stimulation

Mice were habituated to head-fixation over 3 days. The right forepaw was tethered to the recording platform with digits 2, 3 and 4 overhanging the platform edge. A force-feedback movement sensor arm (Aurora Scientific, Dual-Mode Lever Arm Systems 300-C) was positioned underneath digit 3. The sensor arm was held in contact with the glabrous skin of digit 3 with constant force throughout the recordings and provided an online monitor of digit movement as well as delivery of tactile stimuli. Brief (2 ms) tactile stimuli were delivered at a pseudo-randomized time interval (between 2 s and 4 s). Paw movement and sensory stimulation were recorded and delivered alongside neuronal recordings at 20 kHz via an ITC18 board (Heka) under the command of IGOR Pro (Wavemetrics) software.

Electrophysiological recordings

Whole-cell recordings were made with 2 mm external diameter borosilicate glass pipettes (Hilgenberg) with a resistance of 5-7 MΩ. Pipettes were filled with intracellular recording solution, in mM: 135 K-gluconate, 4 KCl, 10 HEPES, 10 Na_2phosphocreatine, 4 MgATP, 0.3 Na_3GTP (adjusted to pH 7.3 with KOH), 2 mg/ml biocytin (Sigma). The brain was covered with Ringer's solution containing, in mM: 135 NaCl, 5 KCl, 5 HEPES, 1.8 $CaCl_2$, 1 $MgCl_2$. An Ag/AgCl ground electrode was placed in the recording chamber. Blind whole-cell recordings were then targeted to L2/3 (subpial depth 100 to 400 µm) and/or L5 (subpial depth 600 to 1000 µm) and performed with a Multiclamp 700b (Molecular Devices) amplifier in current clamp mode at 20 kHz via an ITC18 A/D board and filtered between 0 and 10 kHz. During dual recordings, pipettes were inserted into separate, neighboring craniotomies. The L2/3 pipette was inserted into the D3 craniotomy normal to cortical surface, while the second pipette was inserted through the second, more lateral craniotomy at 45 degrees from vertical to target L5. The recording depths reported in Figure 1 that were not identified with biocytin staining were calculated by triangulation using the angle of the pipette and distance from the pial surface measured by the micromanipulator reading. Intrinsic membrane properties were measured with current injection performed soon after break-in. The V_m was not corrected for the liquid junction potential.

Histological processing

Mice were transcardially perfused with 4% paraformaldehyde (PFA) under deep urethane anesthesia (2.5 g per kg of body weight). The brains were fixed in 4% PFA for at least 12 hours and then placed in phosphate buffer until further processing. 100 µm coronal slices were made using a Leica VT1000 S vibrating microtome. Next, slices were stained for cytochrome oxidase and then for biocytin using an ABC kit (Vectastain). Stained slices were mounted in Moviol and stored in the fridge at 4°C. Neurolucida (MicroBrightField) software was used to reconstruct and photograph stained neurons.

Data analysis

Data were analyzed using custom written scripts in IGORpro (Wavemetrics) and Matlab (MathWorks). All data were statistically analyzed using non-parametric tests, paired data with a Wilcoxon signed rank test and unpaired data with a Wilcoxon rank sum test. Statistical tests are within the same layer across different states (e.g. L2/3 Q versus L2/3 M or L5 QQ versus L5 QM) and across layers within the same state (e.g. L2/3 Q versus L5 Q) but not across layers in different states (e.g. L2/3 Q versus L5 M).

Input resistance

–100 pA, 100 ms current pulses were used to test for input resistance soon after break-in. The change in V_m due to access resistance during input resistance measurements was subtracted from the V_m off-line (Crochet and Petersen, 2006). Access resistance was calculated using an exponential fit of the V_m from a 2 ms period after the start of current injection. The difference in V_m between the baseline and the time point at which the fit crossed the onset time of current injection was taken as the access resistance.

After-hyperpolarization

The after-hyperpolarization (AHP) was calculated as the difference between the baseline V_m at 150 to 50 ms before current injection and the most negative peak in the 100 ms after current injection. The baseline was measured as the mean V_m throughout baseline period, the peak was measured as the mean V_m ± 0.5 ms around the peak AHP.

Behavioral state classification

Moving and quiet periods were selected based on the digit movement signal ($digit_{mov}$). Movement onsets and offsets were detected by thresholding the rectified first derivative ($digit_{FD}$) of the digit movement signal (the $digit_{mov}$ was smoothed using a moving average with a 50 ms window before calculating the first derivative). We used a low threshold (~0.5–2 SD) to reliably detect even small/short movements. In some cases this low threshold resulted in the detection of multiple movement onsets/offsets during long digit movements. To extract only one movement onset and offset in these cases we combined

all onsets/offsets that were less than 500 ms apart and kept only the first onset and last offset. Using these detected movement onsets/offsets we then split the data into quiet and moving epochs of 2 to 4 s duration (see below). To have a clean separation between quiet and moving states we excluded quiet periods that were followed or preceded by a moving state by less than 1 s.

Resting/moving analysis

The detected quiet and moving periods were split into 2 s long epochs to characterize the V_m properties (mean, SD, correlation etc.) shown in Figures 2 and 3. The mean number of epochs/cell was 110.51 ± 10.84 for quiet epochs and 19.45 ± 2.26 for moving epochs. We detected AP thresholds by peaks in the third derivative of the V_m and removed APs from the V_m when analyzing the subthreshold characteristics of the V_m. To characterize the frequency spectrum of the V_m we calculated the fast Fourier transform (FFT) of the baseline subtracted V_m using the FFT function in Matlab. The power of the FFT at low frequencies was measured as the area under the FFT between 1–5 Hz. Cross correlation analysis between pairs of cells was made after the V_m had been baseline subtracted and normalized by the SD. The coherence between pairs of cells was calculated using:

$$Cxy(f) = \frac{|Sxy(f)|^2}{Sxx(f) * Syy(f)}$$

with Sxx and Syy being the power spectra of the two V_m's and Sxy the cross-spectrum. The analysis shown in Figure 2H was done for the entire dataset, i.e., without splitting the data into quiet and moving periods. Here the average V_m value of the depolarized membrane state (Max V_m) was estimated by averaging the 10% most depolarized V_m values.

Slow depolarizing events analysis

To characterize the depolarizing events during quiet periods we selected 4 s long quiet epochs. To detect the onsets and offsets of the depolarizing events (Figure 4A) we smoothed the V_m (25 ms moving average), and thresholded the smoothed V_m at 25–30% of the distance (V_m range) between the Min V_m (the V_m value of the hyperpolarized membrane state) and the Max V_m (the V_m

value of the depolarized membrane state). Min/Max V_m were calculated from the mean 5% of the most hyperpolarized/depolarized V_m values. We included only events with a duration > 100 ms and an average V_m between onset and offset larger than 60% of the V_m amplitude. Furthermore, we excluded events that were preceded by another depolarizing event by less than 100 ms. To calculate the grand average of the onsets/offsets of the depolarizing events we aligned all events to threshold crossing. To estimate the latency between the L2/3 and L5 cell pair at the onset/offset of depolarizing events we fitted each V_m around the onset/offset (± 100 ms) with a sigmoidal function. The latency was then estimated from the time difference at the 5% level of the sigmoidal fits. We included only onsets/offsets in which the fits of both L2/3 and L5 had a goodness-of-fit > 0.6. To characterize the average frequency and duration of slow depolarizing events (Figure S1) we thresholded the V_m as described above. We then merged threshold crossings that were less than 50 ms apart to avoid that large but transient fluctuations during slow depolarizing events were counted as separate events. The frequency of the slow depolarizing events was then given as the number of threshold crossings per second.

Spike triggered averaging

APs were aligned to their peak V_m value time point and separated into two groups: quiet and digit movement. The gradient of a linear fit of the V_m between 22 ms and 2 ms prior to the peak of AP was used to measure the change in V_m prior to a spike (Figure 3).

Spike burst analysis

To analyze whether spikes occurred in bursts we defined the start of a burst as the time when the inter-spike interval between two consecutive spikes was shorter than 10 ms and the burst ended when the inter-spike interval was longer than 15 ms.

Movement onset analysis

To analyze the neuronal responses around the start of a digit movement we detected movement onsets using the method described above. In this

analysis we included all movements, irrespective of their amplitude and duration. The latency between the $digit_{mov}$ and V_m was then estimated by the lag of the peak in the cross correlogram between the $digit_{mov}$ and V_m around the movement onset (–200 ms to 100 ms). The change in V_m variance after movement onset was estimated by calculating the variance of the V_m in a 200 ms window across trials before (–600 to –400 ms) and around the peak after movement onset (~50 to 250 ms, gray shaded areas in Figure 5E).

Tactile response analysis

The onsets of tactile stimuli were used as triggers to study tactile-evoked responses. To classify the behavioral state during tactile stimulation we calculated the amplitude/maximum of the $digit_{mov}$ in a window 300 ms before and 300 ms after stimulation. Using these two measurements we then classified each trial into three categories: quiet-quiet = no movements before and after tactile stimulation, quiet-moving = no movements before but movements after tactile stimulation, moving-moving = movements before and after stimulation. Trials with movements before but not after sensory stimulation were excluded from the analysis. No movement was defined as amplitudes < 1.5*median of all amplitudes and movements were defined as amplitudes > 2.5*median of all amplitudes.

The amplitude of tactile responses (Figures 6E and 7D) was estimated as the difference between the V_m at the stimulus onset (pre-stimulus, 0 ms) and the V_m at the peak of the response. To calculate the trial-by-trial correlation between the tactile-evoked responses of simultaneously recorded cell pairs (Figures 6J and 6K) we calculated the Pearson correlation coefficient between the response amplitudes of both cells. The latency (Figure 6I) was estimated by fitting a sigmoidal function to the average evoked response between stimulus onset and the peak of the response. The time at which the fit crossed 3% of the amplitude was used as a measure of latency.

The tactile-evoked response reversal potential (V_{rev}) was measured using two complementary methods. First, V_{rev} was estimated by linear regression of the amplitude versus the pre-stimulus V_m relationship. For this we fitted a line into the amplitude versus pre-stimulus V_m data and extracted

V_{rev} as the pre-stimulus V_m for which the amplitude was 0 from the fitted line (Figure S7D). In addition, we were able to estimate V_{rev} by the peak of the averaged tactile-evoked response (Figure S7C). This method resulted in almost exactly the same estimates of V_{rev}, as compared to the line-fitting method (Figure S7E, correlation = 0.97, p = 0, mean difference between fit and peak = 1.00 ± 0.15 mV).

The tactile-evoked spiking response (Figure 6F) was calculated by measuring the firing rates in a 100 ms window after stimulus onset (0–100 ms) and by subtracting the baseline firing rate (baseline firing rate was estimated in a 100 ms window before stimulus onset). To calculate the evoked spiking response in the late phase of the tactile response (Figure 7G) we measured the firing rate in the window between 300 and 400 ms after stimulus onset and subtracted the baseline firing rate. To show the relationship between the evoked firing rates and the distance between AP threshold and V_{rev} (Figure 6H) we measured the firing rate in the 100ms window after stimulus onset.

The average V_m during the pre-stimulus phase (Figure 7E) was calculated in a 100 ms window before stimulus onset (from –100 ms to 0 ms), and the average V_m of the late phase (Figure 7F) was calculated between 300 and 400 ms after stimulus onset.